JOURNAL OF APPLIED CRYSTALLOGRAPHY

ISSN 1600-5767

Chord-length distributions cannot generally be obtained from small-angle scattering

Cedric J. Gommes,[a]* Yang Jiao,[b] Anthony P. Roberts[c] and Dominique Jeulin[d]

[a]Department of Chemical Engineering, University of Liège B6A, Allée du six Août 3, B-4000 Liège, Belgium, [b]Materials Science and Engineering, Arizona State University, Tempe, AZ 85287, USA, [c]School of Mathematics and Physics, University of Queensland, Brisbane, QLD 4072, Australia, and [d]MINES ParisTech, PSL – Research University, CMM – Centre for Mathematical Morphology, 35 rue St Honoré, Fontainebleau, F-77300, France. *Correspondence e-mail: cedric.gommes@uliege.be

Received 2 November 2018
Accepted 30 November 2019

Edited by G. J. McIntyre, Australian Centre for Neutron Scattering, Australia

Keywords: small-angle scattering; chord-length distributions; penetrable spheres; Poisson mosaic.

The methods used to extract chord-length distributions from small-angle scattering data assume a structure consisting of spatially uncorrelated and disconnected convex regions. These restrictive conditions are seldom met for a wide variety of materials such as porous materials and semicrystalline or phase-separated copolymers, the structures of which consist of co-continuous phases that interpenetrate each other in a geometrically complex way. The significant errors that would result from applying existing methods to such systems are discussed using three distinct models for which the chord-length distributions are known analytically. The models are a dilute suspension of hollow spheres, the Poisson mosaic and the Boolean model of spheres.

1. Introduction

Small-angle scattering (SAS) data analysis is challenging for two reasons. The first difficulty is that a scattering pattern is mathematically equivalent to a two-point correlation function, which is an incomplete characterization of a structure (Gommes *et al.*, 2012). The second difficulty stems from the variety and geometrical complexity of the structures investigated by SAS, which calls for versatile – and occasionally non-intuitive – descriptors (Serra, 1982; Torquato, 2002; Ohser & Mücklich, 2000). The concept of chord-length distribution (CLD) is one such descriptor. In addition to their geometrical interest, CLDs are physically relevant to radioactive processes (Dirac, 1943) as well as to a variety of phenomena happening in porous materials in the Knudsen regime (Levitz, 1993).

Methods are described in the SAS literature to derive CLDs from scattering data, but they are based on equations with stringent conditions of validity. Namely, one of the phases of the investigated material has to consist of spatially uncorrelated and disconnected convex regions. For colloidal suspensions, these conditions are often reasonably met. However, this is not the case for a wide variety of materials investigated by SAS, the structures of which consist of co-continuous phases that interpenetrate each other in a geometrically complex way. Examples of such structures are found in porous materials, semicrystalline or phase-separated polymers, *etc*. The purpose of this paper is to discuss and illustrate with theoretical examples the errors to be expected when SAS is used to determine chord-length distributions of such materials.

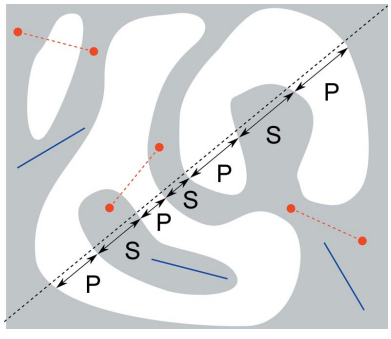

2. Theory

Fig. 1 illustrates a few geometrical concepts related to chord-length distributions using the example of a porous material with solid and pore phases (respectively designated with subscripts S and P), but the same concepts apply to any biphasic system. In order to understand the limits of the structural information that can be obtained from scattering, it is conceptually helpful to think of all structural descriptors as a hierarchy (Matheron, 1967; Torquato, 2002). In that hierarchy, the crudest information one can have is the volume fractions of the pore and solid phases ϕ_P and ϕ_S. These are one-point characteristics because they are equal to the probability that any randomly chosen point belongs to the pores or the solid, respectively. The hierarchy is continued with two-point characteristics such as the covariance $C_{SS}(r)$, which is defined as the probability that any two points at distance r from one another belong to the solid (see Fig. 1). We also define the pore covariance $C_{PP}(r)$ and the pore–solid cross-covariance $C_{SP}(r)$. However, in the case of a two-phase system all the two-point functions are equivalent because they can be expressed in terms of the Debye correlation function:

$$\gamma(r) = \left[C_{SS}(r) - \phi_S^2\right]/\left(\phi_S - \phi_S^2\right). \quad (1)$$

The covariances are occasionally referred to as two-point correlation functions or simply correlation functions.

The hierarchy of structural descriptors is continued to higher orders: three-point correlation functions are defined as the probability for the vertices of randomly positioned triangles to belong to specific phases; four-point functions are defined similarly with tetrahedra, *etc*. Each of these descriptors convey a specific type of geometrical information that lower-order descriptors are blind to (Aubert & Jeulin, 2000; Jiao *et al.*, 2009). A structure is comprehensively characterized if all its n-point correlation functions are known. In the case of small-angle scattering, the hierarchy is interrupted at two-point functions because the measured scattering intensity is the Fourier transform of the Debye correlation function $\gamma(r)$ (Guinier & Fournet, 1955; Porod, 1982; Sivia, 2011). As a consequence, no structural characteristic of order higher than two can be measured by SAS, unless geometrical assumptions are made about the structure. This notably applies to chord-length distributions, because they are concerned with the probability that entire segments – containing an infinite number of points – belong to specific phases.

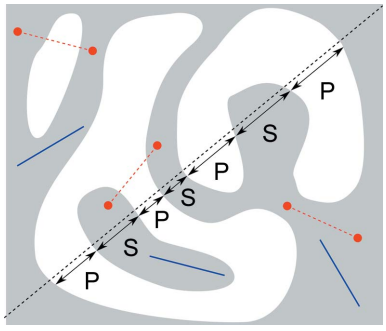

Figure 1
Sketch of a porous material as a general example of biphasic structure, with the solid (S) in grey and pores (P) in white. The red dashes and dots are events that contribute to the covariance $C_{SS}(r)$; the blue segments are events that contribute to the lineal-path function $L_S(r)$, and the black line intersecting the structure is used to define the solid and pore chords.

The geometrical definition of chord lengths is sketched in Fig. 1: a line is drawn randomly through a porous material and solid and pore chords are, respectively, defined as the segments intersecting phases S and P. Their mean lengths l_S and l_P can be calculated from the two-point functions because they quantify how often one crosses an interface, on average, when travelling along the line. As expected, this is related to how often two points close to each other belong to different phases, that is to the small-r values of the cross-covariance $C_{SP}(r)$. In the isotropic case, the actual relation is (Dirac, 1943)

$$l_{S/P} = 4\phi_{S/P}/a_{SP}, \quad (2)$$

where the subscripts S/P highlight that the equation applies both to the solid and to the pore phase. In equation (2), a_{SP} is the specific area of the solid/pore interface, which is obtained from the correlation function as

$$a_{SP} = -4\phi_S\phi_P\gamma'(0). \quad (3)$$

Here the prime denotes the first derivative (Debye *et al.*, 1957).

The chord-length distribution function $g_S(r)$ [or $g_P(r)$] is defined such that the probability for finding a solid (or a pore) chord with length between r and $r + dr$ is given by $g_S(r)\,dr$ [or $g_P(r)\,dr$]. Unlike the mean chord lengths, the distributions $g_S(r)$ and $g_P(r)$ are high-order structural descriptors because they are concerned with the probability that entire segments – containing an infinite number of points – belong to specific phases. Yet, chord-length distributions are often discussed in the small-angle scattering literature (Guinier & Fournet, 1955; Glatter & Kratky, 1982; Feigin & Svergun, 1987; Gille, 2000). The discussion is based on the following formula:

$$g(r) = l\gamma''(r), \quad (4)$$

where the double prime denotes the second derivative and l is a normalization constant having the dimension of a length. Numerical methods have also been developed to invert equation (4) and calculate chord-length distributions from scattering patterns, for both isotropic (Burger & Ruland, 2001) and anisotropic structures (Stribeck, 2001). As a consequence of Babinet's principle, scattering methods cannot discriminate between two phases, which explains why equation (4) cannot be specific about whether it applies to the solid or the pore chords.

In spite of warnings in textbooks – *e.g.* Porod mentioning 'serious difficulties' when applying the concept of chords to 'complicated cases, such as hollow or composite particles, or densely packed systems' (Porod, 1982) – many users of equation (4) seem unaware of its very limited range of validity. The classical derivation of this equation – *e.g.* Guinier & Fournet (1955, Section 2.1.2.4), Glatter & Kratky (1982, Section III.A) or Feigin & Svergun (1987, Section 2.4.3) – considers small-angle scattering by a single particle, which is

equivalent to assuming that particles are spatially uncorrelated. Moreover, the derivation implicitly assumes that the particles are convex. Equation (4) was also derived on more general grounds by Méring & Tchoubar (1968, Section 2.1) in the particular case where all the chord lengths of one of the phases are equally probable. Because the geometrical significance of the latter assumption is unclear, we find it preferable to discuss the validity of equation (4) based on the concept of lineal paths (see Fig. 1).

The lineal-path function $L_S(r)$ [or $L_P(r)$] is a structural descriptor defined as the probability for a randomly positioned and oriented segment of length r to belong entirely to phase S (or P). Contrary to correlation functions, lineal-path functions have a direct relation to CLDs, namely

$$g_{S/P}(r) = \frac{l_{S/P}}{\phi_{S/P}} L''_{S/P}(r), \tag{5}$$

which applies independently to both phases S and P, without any geometrical assumption. This is a classical result of theoretical materials science (Matheron, 1967) and a self-contained derivation is given by Torquato & Lu (1993). Note that lineal-path functions are distinctly different from correlation functions because lineal paths demand that all the points of the segment belong to the considered phase, not only its two end points (see Fig. 1). In the case of convex regions the lineal-path and correlation functions coincide because convexity ensures that an entire segment is embedded in one region if its end points belong to it. Moreover, if the convex regions are spatially uncorrelated the correlation function is a constant for distances larger than the linear size of the individual regions, so that the second derivative in equation (4) vanishes. It is only if these two conditions are met – convex and uncorrelated regions – that equation (4) follows from equation (5) for the considered phase.

3. Three examples

3.1. Hollow spheres

To illustrate the importance of convexity for the validity of equation (4) we shall first consider the case of a dilute suspension of hollow spherical particles, for which the second derivative $\gamma''(r)$ of the Debye correlation function and the solid chord-length distribution $g_S(r)$ can be calculated independently of each other.

The Debye correlation function $\gamma(r)$ of a dilute suspension is proportional to the geometrical covariogram $K(r)$ of the particles, defined as the volume of the intersection of a particle with a copy of itself translated by a distance r (Glatter & Kratky, 1982; Serra, 1982) A hollow sphere with inner and outer radii R_i and R_o, respectively, can be seen as the intersection of the outer sphere with the complementary of the inner sphere. The covariogram can therefore be calculated as

$$K(r) = K_i(r) + K_o(r) - 2K_{oi}(r), \tag{6}$$

where $K_o(r)$ and $K_i(r)$ are the geometrical covariograms of spheres with radii R_o and R_i, respectively, and $K_{oi}(r)$ is the intersection volume of two spheres of radii R_o and R_i at a distance r from one another.

The covariograms $K_i(r)$ and $K_o(r)$ are calculated in the usual way, with the following formula that applies to a sphere of radius R and volume $V = 4\pi R^3/3$, namely

$$K(r) = V\left(1 - \frac{r}{2R}\right)^2\left(1 + \frac{r}{4R}\right) \tag{7}$$

for $r \le 2R$, and $K(r) = 0$ for $r > 2R$. As for the function $K_{io}(r)$, one has to consider several ranges of r. For $r < R_o - R_i$ the smallest sphere fits entirely in the largest so that

$$K_{io}(r) = \tfrac{4}{3}\pi R_i^3. \tag{8}$$

For $R_o - R_i \le r < (R_o^2 - R_i^2)^{1/2}$ the intersection volume can be decomposed into two spherical caps, which leads to

$$K_{io}(r) = \tfrac{4}{3}\pi R_i^3 - \tfrac{1}{3}h_i(3R_i - h_i) + \tfrac{1}{3}h_o(3R_o - h_o) \tag{9}$$

with

$$h_i = \frac{(R_i + r)^2 - R_o^2}{2r} \quad \text{and} \quad h_o = \frac{R_i^2 - (R_o - r)^2}{2r}. \tag{10}$$

For $(R_o^2 - R_i^2)^{1/2} \le r < R_o + R_i$, a similar procedure leads to

$$K_{io}(r) = \tfrac{1}{3}h_i(3R_i - h_i) + \tfrac{1}{3}h_o(3R_o - h_o) \tag{11}$$

with

$$h_i = \frac{R_o^2 - (R_i - r)^2}{2r} \quad \text{and} \quad h_o = \frac{R_i^2 - (R_o - r)^2}{2r}. \tag{12}$$

Finally, for $R_o + R_i \le r$ the two spheres do not touch each other so that $K_{io}(r) = 0$. The Debye correlation function is then obtained as

$$\gamma(r) = \frac{K(r)}{4\pi(R_o^3 - R_i^3)/3}, \tag{13}$$

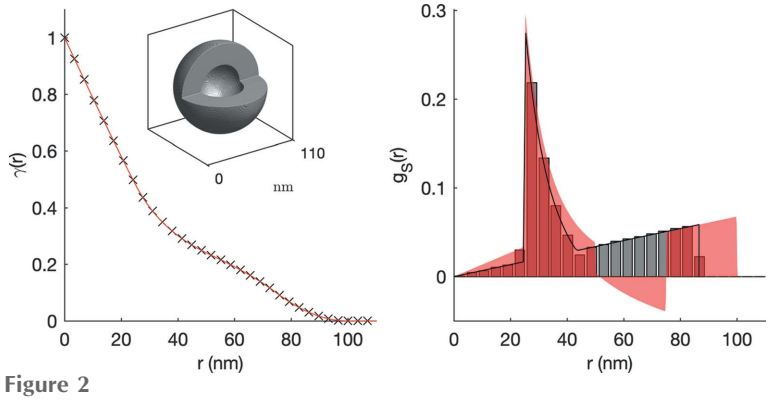

Figure 2
(Left) Debye correlation function $\gamma(r)$ of a hollow sphere with outer radius $R_o = 50$ nm and inner radius $R_i = 25$ nm. The solid red line is the analytical expression and the crosses are obtained numerically from the discretized hollow sphere in the inset. (Right) Solid chord-length distribution $g_S(r)$ of the discretized hollow sphere (bars) compared with the second derivative $\gamma''(r)$ (red shading); the solid black line is the analytical expression of $g_S(r)$ given by Gille [2000, equation (13)].

where the denominator is the volume of the hollow sphere.

The Debye correlation function $\gamma(r)$ of the dilute suspension of hollow spheres and its second derivative $\gamma''(r)$ are both plotted in Fig. 2 (left and right). In the same figure, the chord-length distribution is shown (right). The histogram is obtained numerically from a hollow sphere discretized on a $256 \times 256 \times 256$ grid (shown in inset), and the solid black line is the exact expression (Gille, 2000). To ascertain the accuracy of the numerical procedure, the correlation function of the discretized hollow sphere (left: crosses) is also compared with the analytical value (left: solid red line).

The second derivative of $\gamma(r)$ differs from $g_S(r)$ in several respects. First $\gamma''(r)$ takes negative values for lengths r between 50 and 75 nm, while solid chords clearly exist in that interval of lengths. Moreover, the longest solid chord in the hollow sphere is the one tangent to the inner sphere, and its length is $2(R_o^2 - R_i^2)^{1/2}$. On the other hand, $\gamma''(r)$ takes non-vanishing values for r as large as $2R_o$. Because the longest chord can be made arbitrarily short by decreasing the shell thickness $R_o - R_i$ while keeping R_o constant, one concludes that $\gamma''(r)$ and $g_S(r)$ are independent quantities.

3.2. Poisson mosaic

The second example we consider is that of the Poisson mosaic, for which the correlation function and the chord-length distributions are known analytically for arbitrary densities (Jeulin, 2000). The model is built in two steps. First a random 3D tessellation of space is created, based on Poisson planes with density λ, which divides space into convex cells [Fig. 3(a)]. As a second step, each cell of the tessellation is independently assigned to the solid phase with probability ϕ_S and to pores with probability $\phi_P = 1 - \phi_S$. Realizations of the model are shown in Figs. 3(b) and 3(c), corresponding to ϕ_S = 0.1 and 0.5, respectively. Higher solid fractions, say $\phi_S = 0.9$, are not shown because of the phase-inversion symmetry of the model: all geometrical properties of the solid at $\phi_S = 0.9$ are statistically identical to those of the pores at $\phi_S = 0.1$, and *vice versa*.

The solid and pore chord-length distributions of the Poisson mosaic are given by the following exponential functions:

$$g_{S/P}(r) = (1 - \phi_{S/P})\pi\lambda \exp\left[-(1 - \phi_{S/P})\pi\lambda r\right], \qquad (14)$$

which are plotted in Figs. 3(b_1) and 3(c_1) for the solid chords, and in 3(b_2) and 3(c_2) for the pore chords, together with CLDs measured on the realizations. The Debye correlation function of the model is also known and is given by

$$\gamma(r) = \exp(-\pi\lambda r), \qquad (15)$$

independent of the volume fractions. An uncritical application of equation (4) would lead to the following CLD:

$$g(r) = \pi\lambda \exp(-\pi\lambda r), \qquad (16)$$

which is distinctly different from the correct result in equation (14) for finite values of $\phi_{S/P}$, as also illustrated in Fig. 3. The difference between the actual pore and solid chord lengths of the Poisson mosaic and those estimated wrongly through equation (4) is also apparent when comparing the mean values, which are shown as vertical lines in the figure.

Interestingly, in the particular case of small values of ϕ_S, equation (4) accurately predicts the CLD of the solid $g_S(r)$ [see Fig. 3(b_1)]. In that case, the structure is a dilute collection of convex solid regions because Poisson polyhedra are convex, so that the conditions of validity of equation (4) are met. On the basis of the phase-inversion symmetry of the mosaic model, the same applies to the pore chord distribution $g_P(r)$ for high values of ϕ_S (not shown). In the case where the two phases have comparable volume fractions, equation (4) does not hold, not even as an approximation.

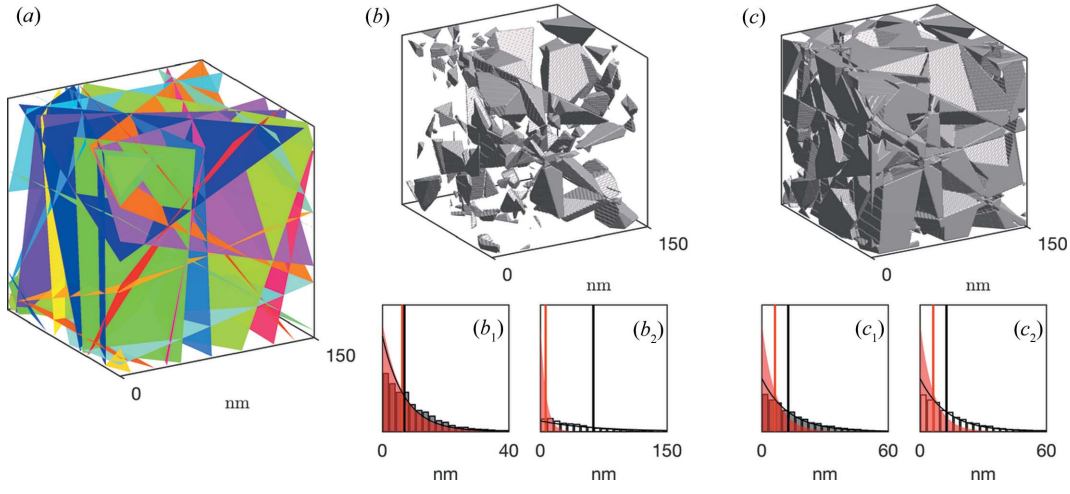

Figure 3
Realizations of a Poisson mosaic model: first a Poisson tesselation is created with density $\lambda = 0.05$ nm^{-1} (a), and each cell is then assigned to the solid phase with probability $\phi_S = 0.1$ (b) and $\phi_S = 0.5$ (c). The corresponding chord-length distributions are shown in (b_1) and (c_1) for the solid, and in (b_2) and (c_2) for the pores. The bars are measured from the realizations, the solid black lines are equation (14) and the red shading shows the distribution estimated from equation (4). The black and red vertical lines are the mean chord lengths calculated from equtions (2) and (4), respectively.

3.3. Boolean model of spheres

To illustrate further the errors to be expected when equation (4) is uncritically applied, we consider now the case of a Boolean model of penetrable spheres. This is a classical model of theoretical materials science (Jeulin, 2000; Torquato, 2002), which is also regularly used in small-angle scattering studies (Sonntag *et al.*, 1981; Gille, 2011; Gommes, 2018). As illustrated in Fig. 4 the model is fully specified by the radius of the spheres R and their density θ. For small densities (Fig. 4) the model yields a structure that consists of almost disconnected particles, which satisfies approximately the conditions of validity of equation (4) for the solid phase. For increasing densities, the spheres overlap each other more often so as to create a complex structure, in which neither the solid nor the pore space is made up of convex regions.

The correlation function and the two chord-length distributions (solid and pore) can be rigorously derived analytically for the Boolean model. In particular, the Debye correlation function is

$$\gamma(r) = \frac{\exp[\theta K(r)] - 1}{\exp(\theta V) - 1}, \tag{17}$$

where V is the volume of individual particles and $K(r)$ is their covariogram, given by equation (7) in the case of spheres. The lineal-path functions are also known analytically (Matheron, 1967; Serra, 1982). In particular, the pore function $L_P(r)$ is a decreasing exponential,

$$L_P(r) = \phi_P \exp[\theta K'(0) r], \tag{18}$$

which results in the pore chord-length distribution

$$g_P(r) = \theta\pi R^2 \exp\left(-\theta\pi R^2 r\right) \tag{19}$$

in the specific case of spheres. The solid lineal-path function $L_S(r)$ of the Boolean model is also know analytically. For any convex grain it is related to the covariance $C_{SS}(r)$ by the following relation:

$$C'_{SS}(r) = L'_S(r) + \frac{1}{1-\phi_S}\int_0^r L'_S(h) C'_{SS}(r-h)\,\mathrm{d}h. \tag{20}$$

Using the covariance in equation (17), this equation can be solved for L_S (and for g_S) via a Laplace transformation (Quintanilla & Torquato, 1996). For the purpose of discussing the validity of equation (4) it is instructive to evaluate the derivative of equation (20) with respect to r, which yields

$$L''_S(r) = C''_{SS}(r) - \frac{1}{1-\phi_S}\left[\int_0^r L'_S(h) C''_{SS}(r-h)\,\mathrm{d}h + L'_S(r) C'_{SS}(0)\right]. \tag{21}$$

It follows from this analytical result that equation (4) cannot be satisfied for the Boolean model because $L''_S(r)$ is proportional to the solid chord-length distribution $g_S(r)$ and $C''_{SS}(r)$ is proportional to $\gamma''(r)$.

To illustrate further the magnitude of the error that would result from applying equation (4) to structures like the Boolean model of spheres, we use it together with equation (17) to predict CLDs and compare them with those measured on realizations of the model for the solid and the pores. This is done in Figs. 4(a_1), 4(b_1) and 4(c_1) for the solid chords, and in Figs. 4(a_2), 4(b_2) and 4(c_2) for the pore chords. In the case of Fig. 4(a_2) many pore chords are longer than the size of the simulation domain, which explains why the CLD estimated from the realization is biased towards short chords compared with the analytical result in equation (19). The mean chord lengths calculated from equation (2) are also shown in the figures and compared with the average value calculated from equation (4). Equation (4) fails to predict the chord-length

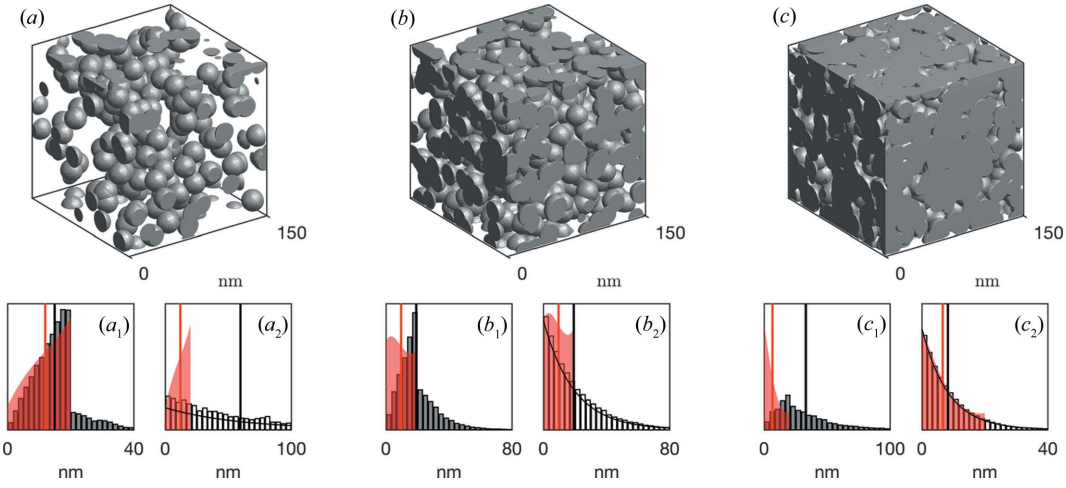

Figure 4
Realizations of a Boolean model of spheres with radius $R = 15$ nm and solid fractions $\phi_S = 0.2$ (a), $\phi_S = 0.5$ (b) and $\phi_S = 0.8$ (c). The corresponding chord-length distributions are shown in (a_1), (b_1) and (c_1) for the solid, and in (a_2), (b_2) and (c_2) for the pores. The bars are measured from the realizations, the solid black lines in the pore chord distributions are equation (19) and the red shading shows the distribution estimated from equation (4). The black and red vertical lines are the mean chord lengths calculated from equations (2) and (4), respectively.

distributions of the Boolean model, as already expected from analytical results.

In two very specific cases, however, equation (4) provides a reasonable approximation. The first is that of small densities [Fig. 4(*a*)], for which the overlap of spheres is so low that the structure almost consists of disconnected convex particles. In that case the solid chord-length distribution is reasonably approximated [Fig. 4(a_1)]. The second case is that of very high densities, for which equation (4) approximates well the pore chord-length distribution [Fig. 4(c_2)]. In that case, it is the pores that are almost disconnected from one another. The pores are not convex because their surface is locally spherical inwards, but they are apparently compact enough for equation (4) to be of practical interest. For all intermediate densities, one would be ill-advised to trust equation (4) and to derive chord-length distributions from small-angle scattering data.

4. Conclusion

Chord lengths are defined as the length of the segments of a line embedded in specific phases of a material (Fig. 1). Their probability distribution provides a general structural descriptor that can be applied to statistically characterize any type of structure, no matter how complex. Because the definition of chords is based on segments, containing an infinite number of points, their length distribution is equivalent to a high-order correlation function. As such, one does not expect chord-length distributions for a general complex material to be measurable by any scattering means, which can only provide second-order correlation functions.

The formula that is widely discussed in the small-angle-scattering literature to calculate chord-length distributions [equation (4)] is based on two strong geometrical assumptions, which are often left implicit in its textbook derivations. Using the general concept of lineal-path function, we show that the formula holds only for a phase consisting of spatially uncorrelated and convex regions. This assumption is often reasonably met for colloidal suspensions, but not for the type of complex and co-continuous structures that one might be tempted to characterize through chord-length distributions. The three examples discussed in the paper – hollow spheres, Poisson mosaic and Boolean model of spheres – show that significant errors result from applying equation (4) when its conditions of validity are not met. The formula might be of practical interest for very dilute pores or very dilute solids. In general, however, one cannot calculate chord-length distributions from small-angle scattering.

Funding information

CJG is grateful to the Funds for Scientific Research (FRS-FNRS, Belgium) for a research associate position.

References

Aubert, A. & Jeulin, D. (2000). *Pattern Recognit.* **33**, 1083–1104.
Burger, C. & Ruland, W. (2001). *Acta Cryst.* A**57**, 482–491.
Debye, P., Anderson, H. R. & Brumberger, H. (1957). *J. Appl. Phys.* **28**, 679–683.
Dirac, P. A. M. (1943). *Approximate Rate of Neutron Multiplication for a Solid of Arbitrary Shape and Uniform Density*, Declassified British Report MS-D-5, part I. Second World War Atomic Energy Research in Britain.
Feigin, L. A. & Svergun, D. I. (1987). *Structure Analysis by Small Angle X-ray and Neutron Scattering.* New York: Plenum Press.
Gille, W. (2000). *Eur. Phys. J. B*, **17**, 371–383.
Gille, W. (2011). *Comput. Struct.* **89**, 2309–2315.
Glatter, O. & Kratky, O. (1982). *Small Angle X-ray Scattering.* New York: Academic Press.
Gommes, C. J. (2018). *Microporous Mesoporous Mater.* **257**, 62–78.
Gommes, C. J., Jiao, Y. & Torquato, S. (2012). *Phys. Rev. E*, **85**, 051140.
Guinier, A. & Fournet, G. (1955). *Small Angle Scattering of X-rays*. New York: John Wiley.
Jeulin, D. (2000). *Stat. Comput.* **10**, 121–132.
Jiao, Y., Stillinger, F. H. & Torquato, S. (2009). *Proc. Natl Acad. Sci. USA*, **106**, 17634–17639.
Levitz, P. (1993). *J. Phys. Chem.* **97**, 3813–3818.
Matheron, G. (1967). *Eléments Pour une Théorie des Milieux Poreux*. Paris: Masson.
Méring, J. & Tchoubar, D. (1968). *J. Appl. Cryst.* **1**, 153–165.
Ohser, J. & Mücklich, M. (2000). *Statistical Analysis of Microstructures in Materials Science*. New York: Springer.
Porod, G. (1982). *Small Angle X-ray Scattering*, editors O. Glatter & O Kratky, pp. 17–51. New York: Academic Press.
Quintanilla, J. & Torquato, S. (1996). *Phys. Rev. E*, **54**, 4027–4036.
Serra, J. (1982). *Image Analysis and Mathematical Morphology*, Vol. 1. London: Academic Press.
Sivia, D. S. (2011). *Elementary Scattering Theory.* Oxford University Press.
Sonntag, U., Stoyan, D. & Hermann, H. (1981). *Phys. Status Solidi A*, **68**, 281–288.
Stribeck, N. (2001). *J. Appl. Cryst.* **34**, 496–503.
Torquato, S. (2002). *Random Heterogeneous Materials*. New York: Springer.
Torquato, S. & Lu, B. (1993). *Phys. Rev. E*, **47**, 2950–2953.